Targeting LRRC15 Inhibits Metastatic Dissemination of Ovarian Cancer

Upasana Ray[1], Deok-Beom Jung[1,2], Ling Jin[1], Yinan Xiao[1], Subramanyam Dasari[3], Sayantani Sarkar Bhattacharya[1], Prabhu Thirusangu[1], Julie K. Staub[1], Debarshi Roy[1,4], Bhaskar Roy[5], S. John Weroha[6], Xiaonan Hou[6], James W. Purcell[7], Jamie N. Bakkum-Gamez[8], Scott H. Kaufmann[9], Nagarajan Kannan[1], Anirban K. Mitra[3], and Viji Shridhar[1]

ABSTRACT

Dissemination of ovarian cancer cells can lead to inoperable metastatic lesions in the bowel and omentum that cause patient death. Here we show that LRRC15, a type-I 15-leucine–rich repeat-containing membrane protein, highly overexpressed in ovarian cancer bowel metastases compared with matched primary tumors and acts as a potent promoter of omental metastasis. Complementary models of ovarian cancer demonstrated that LRRC15 expression leads to inhibition of anoikis-induced cell death and promotes adhesion and invasion through matrices that mimic omentum. Mechanistically, LRRC15 interacted with β1-integrin to stimulate activation of focal adhesion kinase (FAK) signaling. As a therapeutic proof of concept, targeting LRRC15 with the specific antibody–drug conjugate ABBV-085 in both early and late metastatic ovarian cancer cell line xenograft models prevented metastatic dissemination, and these results were corroborated in metastatic patient-derived ovarian cancer xenograft models. Furthermore, treatment of 3D-spheroid cultures of LRRC15-positive patient-derived ascites with ABBV-085 reduced cell viability. Overall, these data uncover a role for LRRC15 in promoting ovarian cancer metastasis and suggest a novel and promising therapy to target ovarian cancer metastases.

Significance: This study identifies that LRRC15 activates β1-integrin/FAK signaling to promote ovarian cancer metastasis and shows that the LRRC15-targeted antibody–drug conjugate ABBV-085 suppresses ovarian cancer metastasis in preclinical models.

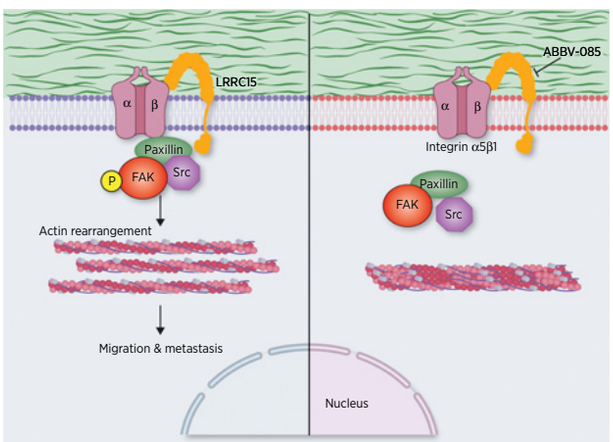

Therapeutic targeting of LRRC15 in ovarian cancer using the antibody-drug conjugate ABBV-085 suppresses FAK activation and reduces metastasis.

Introduction

Widespread peritoneal dissemination at the time of diagnosis is a hallmark of ovarian cancer (1). Peritoneal dissemination and attachment of ovarian cancer to the mesothelium (2) culminates predominantly in omental and bowel metastasis, resulting in malignant bowel obstruction (MBO; ref. 3), which is the major cause of mortality (4) and a common problem in recurrent disease. Despite advances in treatment, the molecular drivers of ovarian cancer dissemination remains poorly defined, thereby impeding development of therapeutic approaches to target bowel metastasis in patients with ovarian cancer (5).

A major challenge is the lack of faithful models that replicate ovarian cancer progression and dissemination to dissect and therapeutically exploit molecular vulnerabilities. The recent report of the first comprehensive molecular characterization of primary ovarian cancer and matching bowel metastatic lesions (mets), identified genes that are differentially expressed. The causal role of any of these candidate genes in ovarian cancer dissemination and bowel metastasis is unclear and needs to be clarified in order to pave the way for future studies

[1]Division of Experimental Pathology and Laboratory Medicine, Mayo Clinic, Rochester, Minnesota. [2]Biomedical Research Center, ASAN Medical Center, Seoul, South Korea. [3]Indiana University School of Medicine-Bloomington, Indiana University, Bloomington, Indiana. [4]Alcorn State University, Lorman, Missisippi. [5]Division of Gastroenterology and Hepatology, Mayo Clinic, Rochester, Minnesota. [6]Department of Oncology, Mayo Clinic, Rochester, Minnesota. [7]Department of Oncology Drug Discovery, AbbVie, South San Francisco, California. [8]Division of Obstetrics and Gynecology, Mayo Clinic, Rochester, Minnesota. [9]Division of Molecular Pharmacology and Experimental Therapeutics, Mayo Clinic, Rochester, Minnesota.

Note: Supplementary data for this article are available at Cancer Research Online (http://cancerres.aacrjournals.org/).

U. Ray and D.-B. Jung contributed equally to the article.

Corresponding Authors: Viji Shridhar, Division of Experimental Pathology and Laboratory Medicine, Mayo Clinic, 200 First Street South West, Rochester, MN55905. Phone: 507-266-2775; E-mail: shridhar.vijayalakshmi@mayo.edu; and Anirban K. Mitra, anmitra@indiana.edu

Cancer Res 2022;82:1038–54

doi: 10.1158/0008-5472.CAN-21-0622

investigating the potential clinical benefit to be gained from targeting these mechanisms, if evidences emerge causally linking them with malignant spread.

Of these genes, a type-I 15-leucine–rich repeat-containing membrane protein encoding *LRRC15* gene was found to be highly represented in bowel mets and our preliminary investigation had revealed its role in peritoneal metastasis and growth (6). LRRC15 located on chromosome 3 at 3q29 is a 581 amino acid containing membrane protein that belong to the LRR superfamily that lack an intracellular signaling domain (7–8) and was reported to be highly expressed on cancer-associated fibroblasts within the active stroma in numerous solid tumors and directly in the epithelial cancer cell compartment of mesenchymal tumors like glioblastoma, sarcomas, and melanoma (9). Previously, LRRC15 has been functionally linked with regulating cell–cell and cell–extracellular matrix (ECM) interactions by likely partnering with a range of ECM proteins including fibronectin, laminin, and collagen IV through its extracellular leucine-rich repeats (10, 11). Increased stromal expression of LRRC15 is reported in multiple solid tumor types including breast, ovarian, and cervical cancers (6, 12–14). Therefore, the objective of our current study was to further investigate the role of and characterize the mechanism(s) through which LRRC15 promote ovarian cancer dissemination and bowel and/or omental metastasis. In this study using multiple ovarian cancer cell lines and xenotransplantation models and a range of functional and molecular assays we have determined a mechanistic link between LRRC15 expression and promotion of ovarian cancer metastasis. We also provide the first preclinical proof-of-concept evidence that LRRC15 expression creates a therapeutic vulnerability that could be targeted using the humanized anti-LRRC15 antibody–drug conjugate (ADC) ABBV-085, to blockade ovarian cancer dissemination and bowel and/or omental metastasis.

Materials and Methods

Reagents

ABBV-085 (anti-LRRC15 humanized IgG1 antibody, consisting of hydrophobic interaction chromatography-enriched E2 in which approximately two antimitotic monomethyl auristatin E (MMAE) payloads are conjugated per antibody through a protease cleavable valine–citrulline (vc) linker, Isotype mAb, and Isotype-vc-MMAE-E2 drug control were received from AbbVie (9). Other reagents and antibodies used were listed in Supplementary Table S1.

Cell culture

Human ovarian cancer cell lines, LP9/TERT-1 mesothelial cells (15), immortalized normal ovarian fibroblast NOF151hTERT and TRS3 stromal cells, immortalized normal ovarian surface epithelial cells VOSE and IOSE523 (16) were maintained as shown in Supplementary Table S2. Patient-derived ascites were obtained with the approval and written informed consent [Institutional Review Board (IRB)–1288–03 to V. Shridhar] through the Mayo Clinic Ovarian SPORE program and in collaboration with the University of Minnesota Cancer Center Tissue Procurement Facility with IRB approval and cultured as mentioned (17, 18). The studies were conducted in accordance with recognized ethical guidelines (e.g., Declaration of Helsinki, CIOMS, Belmont Report, U.S. Common Rule).

Generation of knockdown and overexpressed stable clones

LRRC15 knockdown (KD) was performed in the OVCAR5 cells with shLRRC15 (Sigma-Aldrich) targeting 3′UTR (Sequence: sh1-GCTATGAAAGAGAGAAGGAAA and sh2-CCAGGTTTCTTCTTCTCTTAA) and stable overexpression of HA-LRRC15 (Sino Biologicals) in OVCAR7 cell line using standard transfection guidelines and reagents.

ITGB1 knockout (KO) OVCAR5 cells were generated using Crispr/cas9 method using single-guide RNA (sgRNA) clone (target site: TTTGTGCACCACCCACAATT, Genecopoeia) using manufacturer protocol.

Spheroid formation assay

OVCAR7 empty vector (EV) control and OVCAR7 LRRC15-overexpressed (OE) and OVCAR5 nontargeted control (NTC) and OVCAR5 sh1 (LRRC15 stable KD) cells were seeded in ultralow attachment 24-well plates (2,500 cells/well) for spheroid formation assay. Spheroids were allowed to form for 6 days and imaged using EVOS FL Auto Imaging System (Life Technologies). At least 3 wells were imaged for each biological replicate. Spheroids were manually quantified.

Anoikis assay

One million OVCAR5 NTC and sh1 cells and OVCAR7 EV-transfected and LRRC15 overexpressed cells were grown in suspension for 0 to 6 days. Cell viability was assessed by MTT assay from the replated cultures grown for 6 days (19) and cell survival ability was analyzed by clonogenic assay (20).

Adhesion to mesothelial cells

LP9/TERT-1 mesothelial cells were grown on 96-well plates. OVCAR5 NTC, sh1/sh2 cells and OVCAR7 EV, LRRC15 cells were prelabeled with 10 mmol/L CellTracker Green (CMFDA) for 45 minutes at 37°C. The labeled cells were washed and 2×10^4 cells per well was added to the mesothelial cells in 4 replicates. After incubation for indicated times, the nonadherent cells were washed and fluorescence was quantified using Scion Image Software (Scion Corp).

Adhesion to fibronectin and other ECM proteins

Each of 2 μg/mL fibronectin, 10 mg/mL poly-L-lysine, 0.1 mg/mL collagen, 1 mg/mL laminin, 0.5 mg/mL vitronectin was added to 96-well plates in 4 replicates and allowed to air dry. Twenty thousand CMFDA-labeled cells per well were seeded on coated plates and after incubation for indicated times, the nonadherent cells were washed, and fluorescence was quantified using Scion Image Software.

Scratch wound-healing assay

The OVCAR5 NTC and sh1 KD cells and OVCAR7 EV and LRRC15 OE cells were scratched with 10 μL pipette tips and replaced with fresh media. Zero-hour/24-hour images were captured using an EVOS inverted microscope (Thermo Fischer Scientific).

Immunoblot analysis

Whole-cell lysates were subjected to immunoblot analysis (21) against antibodies– LRRC15, cleaved PARP1, cleaved caspase-3, ITGB1, phospho–focal adhesion kinase (FAK)^{y397}, FAK, MMP2, PCNA, GAPDH, and β-actin, visualized using fluorophore-conjugated secondary antibodies (LICOR) by LI-COR OdysseyFc Imaging System as described (19). Details of the antibodies used were listed in Supplementary Table S1.

Three-dimensional invasion assay

The Three-dimensional (3D) culture model mimicking the surface layers of the omentum was assembled in fluoroblock transwell inserts with 8 μm pores using normal omental fibroblasts (NOF) and human

peritoneal mesothelial cells (HPMC), isolated from human omentum, as described previously (22). Briefly, NOFs (4×10^3) mixed with 1.82 μg of collagen type 1 in 50 μL DMEM were seeded in transwell fluroblock inserts (8 μm pores, 0.6 cm^2) and incubated at 37°C for 5 hours. Thereafter, 5×10^4 HPMCs in 50 μL DMEM were seeded on top of this basement membrane like layer to form a confluent monolayer resembling the mesothelium. CMFDA-labeled OVCAR5 NTC or sh1 cells and OVCAR7 EV or LRRC15 OE (5×10^4/500 μL) cells were seeded in serum-free DMEM on the 3D culture and 700 μL of DMEM with 10% FBS was added in the lower chamber to serve as a chemoattractant. Invasion was stopped after 8 hours by fixing with 4% paraformaldehyde. The invaded fluorescent ovarian cancer cells on the lower surface of the inserts were imaged (5 fields/insert) using the EVOS FL auto microscope (Life Technologies) and counted.

3D adhesion assay

The 3D culture model mimicking the surface layers of the omentum was assembled in 96-well Black/clear-bottom tissue culture plates as described in the 3D Invasion assay. Briefly, 2×10^3 NOFs along with 0.91 μg of collagen type 1 was added in each well and overlayed with 2.5×10^4 HPMCs. CMFDA-labeled NTC/sh1 and EV/LRRC15 OE (2.5×10^4/50 μL) cells were seeded on the 3D culture. Cells were allowed to attach for 30 minutes, and the total fluorescence was quantified using a SynergyH1 plate reader (BioTek). The wells were washed with PBS to remove the nonadherent cells and the residual fluorescence was measured to quantify the percentage of adherent cells.

In vivo adhesion assay

Six-week-old female NOD/SCID gamma (NSG) mice (3 mice/group) were injected with the CMFDA fluorescent-labeled LRRC15 short hairpin RNA (shRNA) or NTC control OVCAR5 cells or LRRC15-overexpressing or EV control OVCAR7 cells intraperitoneally (1 million cells in 0.5 mL PBS). Mice were euthanized 3 hours postinjection. Omentum and peritoneum were dissected and washed with PBS to remove nonadherent cells. The attached cancer cells were dissociated by incubating in trypsin at 37°C with gentle oscillation. The dissociated cells were collected, and their fluorescence was quantified using a SynergyH1 plate reader.

Immunoprecipitation assay

Equal amounts of cell lysates were incubated with anti-ITGB1 or anti-LRRC15 separately for 24 hours at 4°C followed by protein A/G-agarose beads addition for 24 hours, processed following the manufacturers' protocol, and was probed for LRRC15 or ITGB1 respectively.

Immunofluorescence imaging

NTC, sh1 OVCAR5 and EV, LRRC15 OVCAR7 cells were seeded on fibronectin-coated cover slips (10 μg/mL) and allowed to attach overnight (21), probed for anti-ITGB1, anti-LRRC15, and anti-vinculin antibodies and captured using Zeiss-LSM 510 confocal microscope.

Flow cytometric extracellular antigen staining

NTC and sh1/sh2 cells were fixed, permeabilized, and probed for primary-tagged anti-ITGB1 and anti-CD44 as discussed (23). The samples were analyzed using a LSR II FACS analyzer (BD Biosciences).

Proximity ligation assay

NTC, sh1 OVCAR5 and EV, LRRC15 OVCAR7 cells were seeded on fibronectin (10 μg/mL)-coated chamber slides and permitted to attach overnight. The cells were processed using the manufacturers' protocol of the Duolink *In Situ* Red Starter Kit where the cells are probed for either rabbit anti-LRRC15 or mouse anti-ITGB1 or both followed by ligation and amplification process and the signal was captured using Zeiss-LSM 510 confocal microscope.

Mouse xenograft model of OVCAR5 cells

5 million cells were injected intraperitoneally into 4 to 5 weeks old, female athymic nude mice. In the posttreatment study model the treatment was initiated 1 week after tumor cell injection and mice were randomized into 3 groups of 5 each, and treatment was continued for 4 weeks. Conversely, in the pretreatment model the mice were randomized into 3 groups of 7 mice each and the treatment was started 3 days prior to tumor cell injection and continued for 2 weeks. Treatment includes ABBV-085, an MMAE-containing ADC (6 mg/kg) and the controls Isotype mAb (6 mg/kg) and Isotype-vc-MMAE-E2 drug control (6 mg/kg) were injected intraperitoneally; eventually all mice were euthanized at day 36. All experimental use of animals will comply with the guidelines of the Institutional Animal Care and Use Committee (IACUC) at the Mayo Foundation following approved protocols.

Patient-derived tumorograft model of ovarian cancer

Fresh tissues were collected from patients with ovarian cancer after consent in accordance with the Mayo Clinic IRB through the Mayo Clinic Ovarian Tumor Repository. Tumor grafts were developed as previously described (24, 25) under the guidelines of IACUC. Briefly, approximately 0.3mL of minced fresh patient tumor was mixed 1:1 with media and intraperitoneally injected into 6 to 8 weeks old female SCID mice. Mice were monitored by ultrasound and treatment was started when tumors reached 0.5 to 1 cm^2. For posttreatment model of PH081, treatment started 2 weeks after tumor injection. Mice were randomized in 3 groups each of 10 and therapy started with i.p. administration of Isotype mAb (6 mg/kg), the Isotype-vc-MMAE-E2 (6 mg/kg), and ABBV-085 (6 mg/kg) for a total of 6 treatments at an interval of 4 days. For the pretreatment model of both PH127 and PH081, similar treatment was administered 3 days prior to the tumor injection followed by another 5 dosages at an interval of 4 days. The tumor mass was assessed weekly by ultrasound; mean of 3 measurements per session for each animal were provided. All experimental use of animals follow approved protocols under the guidelines of the IACUC at the Mayo Foundation.

IHC

IHC studies were performed on formalin fixed deparaffinized sections as previously described (19). Expression analysis in the xenograft tumor tissue was probed against Ki-67. IHC study for LRRC15 expression was performed in the primary tumor and their autologous omental mets from patients with ovarian cancer and on patient tissue microarray (TMA) containing 27 clear cell, 28 endometrioid and 8 high grade serous tumors as discussed in (6). TMA slide was scanned on the Aperio ScanScope AT Turbo brightfield instrument (Leica Biosystems) at 40x magnification and a resolution of 0.25 μm per pixel. LRRC15 expression level was scored for intensity and the data was plotted.

Statistical analysis

All investigation was performed in triplicates for 3 independent experiments unless mentioned otherwise. The results were expressed as mean ± SD. Significant changes (*, $P < 0.05$; **, $P < 0.01$) were determined by two-sided unpaired *t* tests, unless otherwise noted.

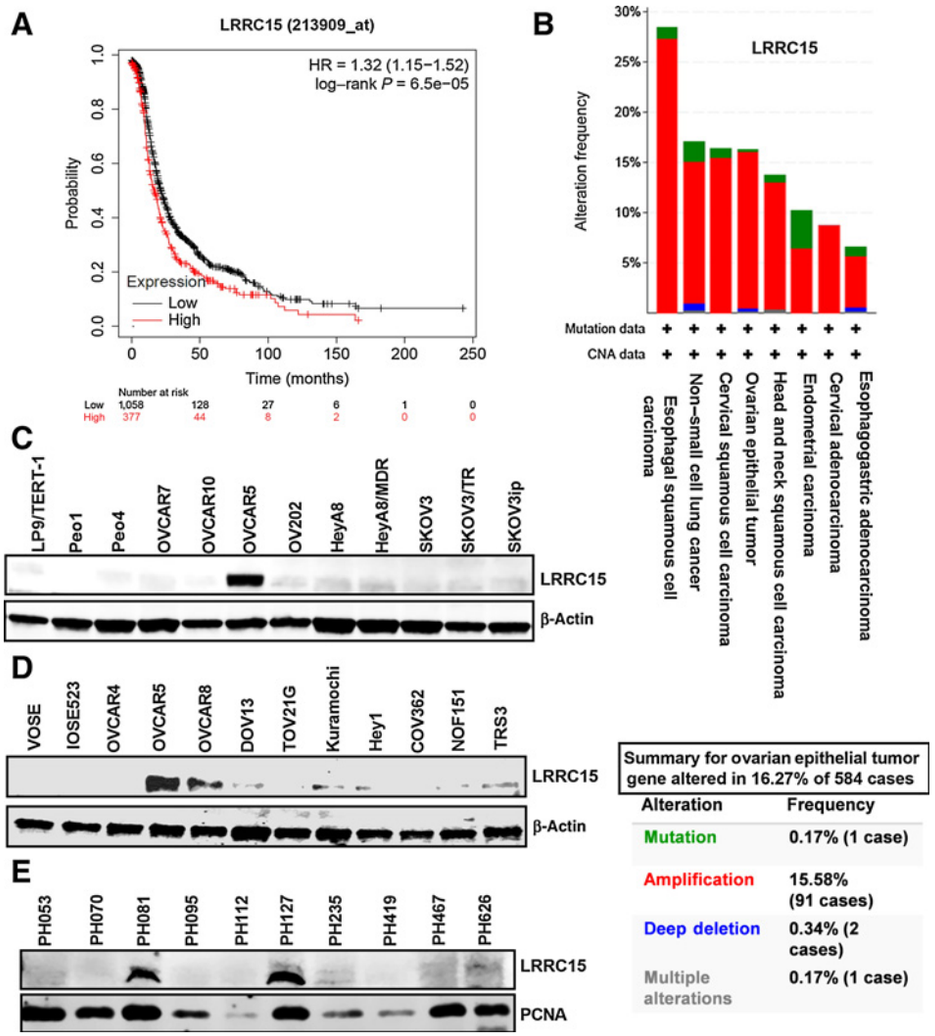

Figure 1.

LRRC15 is associated with ovarian cancer. **A,** Kaplan–Meier progression-free survival analysis shows high LRRC15 expression is associated with worse progression-free survival in a cohort of 1,436 patients with ovarian cancer. **B,** TCGA analysis of LRRC15 expression in several cancer types along with the percent gene altered as evaluated in the ovarian epithelial tumor. **C** and **D,** Immunoblot analysis of LRRC15 in ovarian cancer cell lines and in the ovarian cancer fibroblast cell lines NOF15hTERT and TRS3 and in the normal ovarian surface epithelial cells VOSE and IOSE523. β-actin was used as loading control. **E,** Western blot analysis of LRRC15 and proliferating cell nuclear antigen (PCNA) expression as control in 10 ovarian cancer PDX tumors.

Results

LRRC15 expression is associated with poor ovarian cancer patient outcome

RNA sequence of bowel met biopsies compared with matching primary tumors in patients with ovarian cancer ($n = 21$) identified LRRC15 gene among few others to be significantly represented at high levels in bowel mets (6). Analysis of LRRC15 expression in patients with ovarian cancer ($n = 1436$) using Kaplan–Meier analysis (**Fig. 1A**) showed higher expression of LRRC15 was significantly associated with adverse outcome. The Cancer Genome Atlas (TCGA) analysis of high-grade serous subtype showed 16% cases with LRRC15 amplification (**Fig. 1B**). Similar to bowel mets (6), LRRC15 was highly expressed in the stroma of omental mets (7/15) compared with autologous primary tumors (Supplementary Fig. S1A), with no significant changes in 6/15 samples (Supplementary Fig. S1B). Additionally LRRC15 expression was determined by IHC on a patient TMA containing 27 clear-cell, 28 endometrioid, and 8 high-grade serous tumors. Patient characteristics were described in Supplementary Table S3. Levels of LRRC15 expression were categorized as no (0), low (1+), moderate (2+), and high (3+) staining and plotted (Supplementary Fig. S1C). Representative triplet sections showing 2+ intensity in the different histologies is shown in Supplementary Fig. S1C. Seven of 27 (26%) clear-cell tumors, 16 of 28 (57%) endometrioid tumors, and 5 of 8 (62.5%) high-grade serous tumors expressed high levels of LRRC15. Expression analysis of LRRC15 in the tumor and stromal compartments in the TMA revealed stromal LRRC15 positive staining in 1 of 7 LRRC15$^+$ (14.2%) clear-cell tumors, 3 of 16 LRRC15$^+$ (18.7%) endometrioid tumors, and 2 of 5 LRRC15$^+$ (40%) high-grade serous tumors (Supplementary Fig. S1D).

LRRC15 expression promotes multiple cellular properties necessary for ovarian cancer dissemination and omental metastasis

Peritoneal metastases is regulated by the ability of ovarian cancer cells to shed from the primary tumor, survive during transit as free-floating single cells or cell aggregates, and subsequently attach to and invade through mesothelial lining of the abdominal cavity to colonize various metastatic sites (26, 27). We, therefore, investigated the role of LRRC15 in this metastatic cascade. Western blot analysis showed that OVCAR5 and 8 cells robustly expressed LRRC15 with Kuramochi, DOV13, Hey1, and TRS3 cells with lower levels of LRRC15 (**Fig. 1C–D**). In contrast, normal ovarian surface epithelial VOSE and IOSE523 cell lines, the normal ovarian fibroblast cell line NOF151hTERT, and the LP9/TERT-1 mesothelial cells were deficient

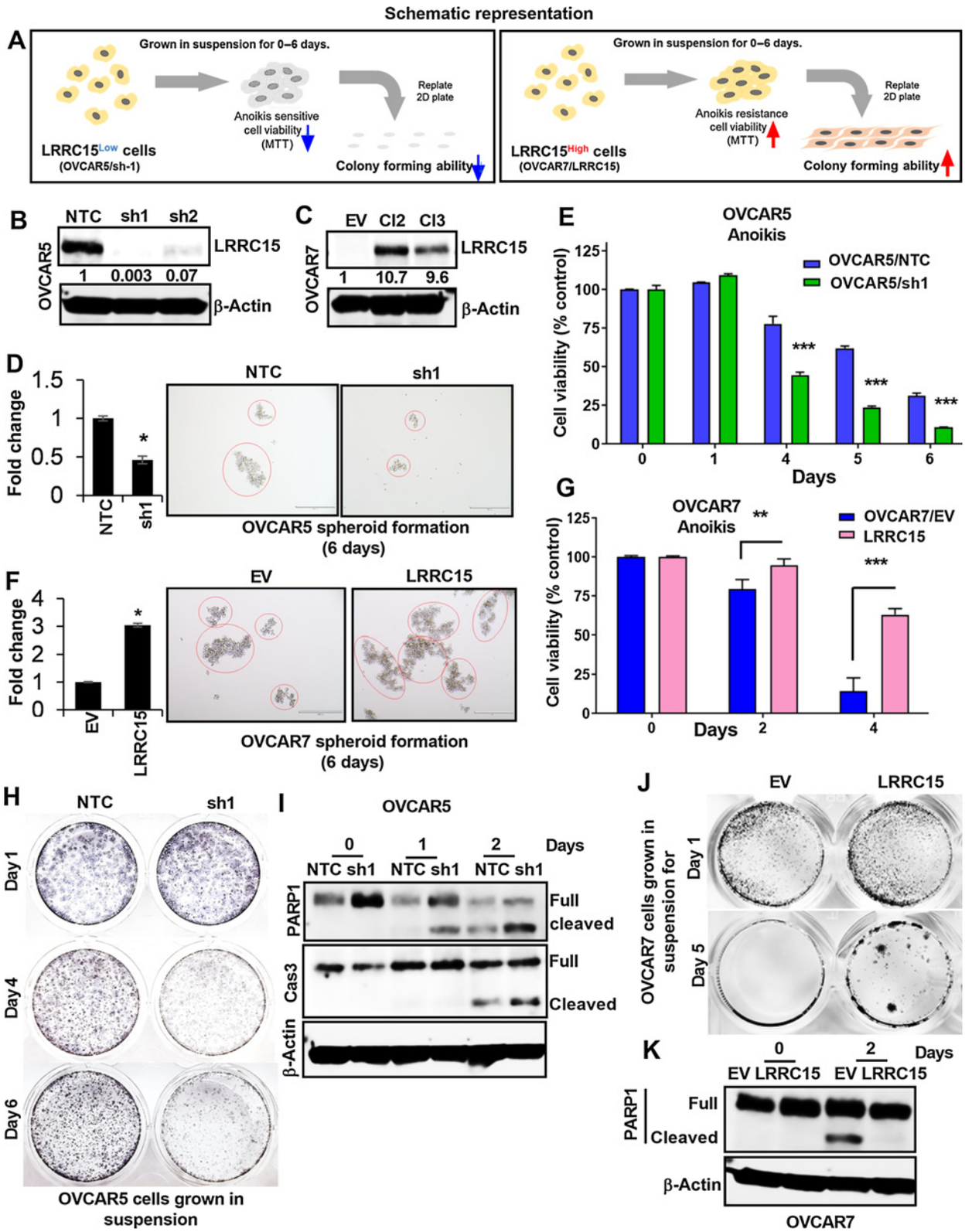
Schematic representation
A
Grown in suspension for 0–6 days.
LRRC15Low cells
(OVCAR5/sh-1)
Anoikis sensitive
cell viability
(MTT)
Replate
2D plate
Colony forming ability
Grown in suspension for 0–6 days.
LRRC15High cells
(OVCAR7/LRRC15)
Anoikis resistance
cell viability
(MTT)
Replate
2D plate
Colony forming ability
B
NTC sh1 sh2
OVCAR5
LRRC15
1 0.003 0.07
β-Actin
C
EV Cl2 Cl3
OVCAR7
LRRC15
1 10.7 9.6
β-Actin
D
Fold change
NTC
sh1
OVCAR5 spheroid formation
(6 days)
E
OVCAR5
Anoikis
OVCAR5/NTC
OVCAR5/sh1
Cell viability (% control)
Days
F
Fold change
EV
LRRC15
OVCAR7 spheroid formation
(6 days)
G
OVCAR7
Anoikis
OVCAR7/EV
LRRC15
Cell viability (% control)
Days
H
NTC
sh1
Day1
Day4
Day6
OVCAR5 cells grown in
suspension
I
OVCAR5
Days
NTC sh1 NTC sh1 NTC sh1
PARP1
Full
cleaved
Cas3
Full
Cleaved
β-Actin
J
EV
LRRC15
OVCAR7 cells grown in
suspension for
Day 1
Day 5
K
Days
EV LRRC15 EV LRRC15
PARP1
Full
Cleaved
β-Actin
OVCAR7

in LRRC15 (**Fig. 1C–D**). Additionally, immunoblot analysis of ovarian cancer patient-derived tumorografts (PDX) showed high expression of LRRC15 in PH127 and PH081 tumors (**Fig. 1E**).

Next, we investigated the role of LRRC15 in ovarian cancer metastasis as described schematically in **Fig. 2A**. We generated KD LRRC15 expression clones in OVCAR5 cells using two different shRNAs (sh1 and sh2) and the NTC as control (**Fig. 2B**), and overexpression clones of LRRC15 in OVCAR7 cell line with no detectable levels of LRRC15 and generated OVCAR7 Cl2/Cl3 (LRRC15 overexpression) or EV (**Fig. 2C**). To mimic the *in vivo* microenvironment, cells were initially cultured on 3D ultralow attachment plates as spheroids for 6 days to assess whether sphere formation depends on LRRC15 expression. LRRC15-expressing OVCAR5 and OVCAR7 OE cells showed significantly more larger spheroids compared with the LRRC15 KD and vector transfected cells respectively (**Fig. 2D** and **F**). Cells were replated under 2D conditions to confirm that LRRC15 overexpressing cells were viable and survived in an environment not attached to ECM using MTT and CFA assays respectively. Interestingly, KD of LRRC15 in OVCAR5 cells led to loss of survival and colony forming ability. The surviving fraction of dissociated single cells replated in 2D tissue culture dishes at clonal densities further suggested that LRRC15 depletion promoted anoikis (**Fig. 2E** and **H**). In contrast OVCAR7/LRRC15 cells showed improved cell viability and colony forming ability compared with controls (**Figs. 2G** and **J**), suggesting LRRC15 overexpression promotes anoikis resistance. Consistent with these results, levels of cleaved PARP1 as determined by immunoblot analysis showed increased expression in OVCAR5 KD cells and decreased expression in OVCAR7/LRRC15 cells compared with their respective controls (**Figs. 2I** and **K**).

To understand the role of LRRC15 in cell–to–cell adhesion and how the altered expression of LRRC15 affects the ability of cancer cells to adhere to mesothelial cells, OVCAR5 and OVCAR7 derivative cell lines were prelabeled with CMFDA and added on top of the LP9/TERT-1 mesothelial cells monolayer. Fluorescence intensity was measured at the indicated time points, which reflect the degree of cancer-cell adhesion to mesothelial cells. We found a significant reduction in the adhesion property of the LRRC15-deficient cells to the mesothelial layer, however the LRRC15-overexpressed cells showed an increased adherence phenotype compared with EV cells (**Fig. 3A–B**). We also assessed the ability of the fluorescently labeled cells to adhere to the omentum surface using the 3D culture model mimicking the surface layers of the omentum (**Fig. 3C**; ref. 22). A significant decrease in the adherence percentage (17%) of OVCAR5 KD cells was observed compared with NTC cells (41.5%, **Fig. 3D** and **E**). In contrast, a significant increase in the adhesion phenomenon under similar assay condition was obtained in the LRRC15/OVCAR7 cells compared with control (**Fig. 3F**). However, no alteration was obtained in the proliferative ability of the either the LRRC15 KD or overexpressed cells compared with their respective controls (Supplementary Fig. S2A–B).

Given that the LRRC15-deficient cells lose their adherence property to the omental layer known to express both fibronectin and vitronectin (28), fluorescently labeled OVCAR5 NTC and sh1 KD cells were seeded on the top of the poly-L-lysine–, collagen 1A1-, fibronectin (FN)-, laminin-, and vitronectin-coated plates for 1 hour and the percentage of adhered cells were counted. Results indicate that KD cells showed a significant reduction in adhesion to fibronectin, collagen1A1, and vitronectin (Supplementary Fig. S2C, 3G), with no significant change in adherence to the poly-L-lysine– and laminin-coated plates. To further validate, we performed an *in vivo* adhesion assay by injecting CMFDA-labeled OVCAR5 KD and NTC cells intraperitoneally into NSG female mice. After 3 hours, mice were sacrificed, omentum and peritonium were dissected, washed with PBS, and adherent cancer cells were dissocated with trypsin. The fluorescence intensity of the dissociated cancer cells was measured to quantify the extent of adhesion. A significant decrease in fluorescence intensity indicative of reduced adherence rate was observed in the KD group of mice compared with the control cohort (**Fig. 3H** and **I**). To confirm we also performed the *in vivo* adhesion assay injecting CMFDA-labeled OVCAR7 LRRC15 OE and EV control cells intraperitoneally in a similar manner as mentioned above and the data revealed significant upregulation in fluorescence intensity suggestive of increased adherence rate observed in the LRRC15 OE group of mice compared with the control cohort (**Fig. 3J**). These results highlight the importance of LRRC15 in ovarian cancer metastatic cascade.

LRRC15 regulates focal adhesion formation in ovarian cancer cells

Activation and clustering of integrins upon binding to ECMs lead to focal adhesion (FA) formation and the complex formation was analyzed in the OVCAR5 and OVCAR7 derivatives when grown on FN-coated plates and immunostained for vinculin and F-actin. Earlier reports establish vinculin as a principal regulator of the FA formations (29–31) and have shown that vinculin downregulation results in reduced adhesion and increased migration compared with vinculin-expressing wild-type cells. In contrast, vinculin overexpression increases the number/masses of FAs and diminished cell motility (32). Confocal imaging against fluorescently tagged vinculin (red) showed larger and numerous FA complexes mostly in the interior of the OVCAR5 sh1 KD cells compared with the smaller and fewer ones towards the periphery of the control cells (**Fig. 4A**). Moreover, the OVCAR7/LRRC15 cells showed redistribution of vinculin colocalizing with F-actin (green) in the periphery of cancer cells compared with EV cells (**Fig. 4B**). Percentage of vinculin-positive cells were calculated in a total of 50 cells per group, which is shown **Fig. 4C**. Together, the results are in agreement with the increased migratory phenotype observed in cells with LRRC15.

Figure 2.

LRRC15 renders cells resistant to anoikis. **A,** Schematic representation of the experimental protocol. **B** and **C,** Immunoblot analysis of LRRC15 expression in OVCAR5 NTC and sh1/sh2 KD cells (**B**) and in the OVCAR7 EV-transfected control cells and Cl2 and Cl3 LRRC15 OE cells (**C**). β-Actin was used as a loading control. Fold change was calculated using the Image J software, normalized to endogenous control, and provided beneath the panel. **D,** 3D-spheroid formation assay was performed for 6 days in OVCAR5 NTC control and LRRC15 sh1 KD cells. Quantification as fold change was provided. **E,** OVCAR5 NTC and sh1 cells spheroids were subsequently transferred into adhesive plates for the indicated time points, followed by MTT assay. The percent cell viability was scored and plotted. Results show the mean ± SEM. **F,** Spheroid formation assay was performed in OVCAR7 EV control and LRRC15 OE cells and is represented as fold change. **G,** Cell viability assay was performed in the mentioned cells for the indicated time points in similar manner. The percent cell viability was plotted with the mean ± SEM. **H,** Colony-forming assay was performed with OVCAR5 NTC and sh1 spheroid culture transferred in 6-well adhesive plates and imaged upon staining with Coomassie blue for the mentioned time points. **I,** Immunoblot analysis of cleaved PARP1 and cleaved caspase-3 levels was performed under similar conditions for days 0 to 2. **J** and **K,** Colony-forming assay and Western blot analysis for cleaved PARP1 was performed in the OVCAR7 EV and LRRC15 overexpressed cells in a similar manner. β-actin used as loading control. **, $P < 0.01$; ***, $P < 0.001$.

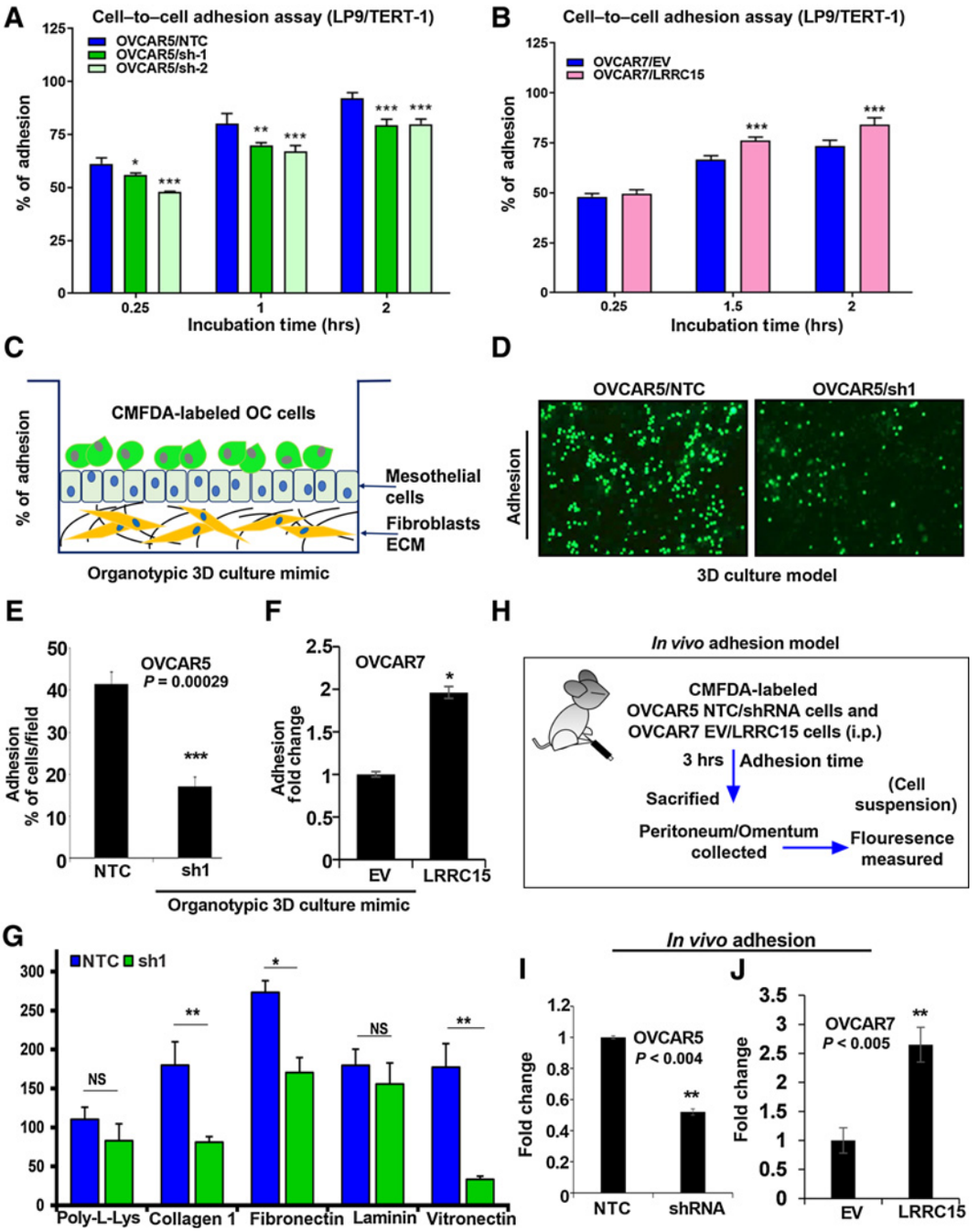

Figure 3.

LRRC15 KD abrogates the adhesion phenomenon in the OC cells. **A** and **B,** OVCAR5 NTC, sh1/sh2 (**A**), and OVCAR7 EV and LRRC15 (**B**) overexpressed cells were prelabeled with fluorescent CMFDA and seeded onto the top of the LP9/TERT-1 mesothelial monolayer culture. hrs, hours. Fluorescent intensity was measured at the mentioned time points, which reflect the percent of cancer cells that gets adhered to the mesothelial layer and the percent cell adherence after normalization was plotted as mean ± SEM. **C,** Schematic representation of the organotypic 3D culture model of the surface layers of the omentum. OC, ovarian cancer. **D,** Representative images of fluorescently labeled NTC and sh1 OVCAR5 cells adhering to the 3D culture model. **E,** The percent adherent NTC and sh1 OVCAR5 cells were measured and plotted as mean ± SEM. **F,** The percent of EV and LRRC15-overexpressing (LRRC15) OVCAR7 cells adhering to the 3D culture was measured and plotted as mean ± SEM. **G,** OVCAR5 NTC and sh1 cells were prelabeled with CMFDA and then seeded onto the top of the culture dishes that were precoated with poly-L-lysine, collagen 1A1, fibronectin, laminin, and vitronectin, respectively. Percent adhered cells were represented as mean ± SEM. **H,** Schematic representation of the *in vivo* adhesion assay in NSG mice model of ovarian cancer. *In vivo* adhesion was performed by intraperitoneal injection of CMFDA-labeled NTC and LRRC15 shRNA OVCAR5 cells or EV and LRRC15 OVCAR7 cells in female NSG mice ($n = 3$/group). After 3 hours, the mice were sacrificed and the peritoneum/omentum tissues were collected, cancer cells dissociated, and fluorescence intensity was measured in the cell suspension. **I** and **J,** The fold change in fluorescent intensity was plotted as a measure of adhesion for NTC vs. LRRC15 shRNA cells (**I**) and EV vs. LRRC15 overexpressing cells (**J**). NS, not significant; *, $P < 0.05$; **, $P < 0.01$; ***, $P < 0.001$.

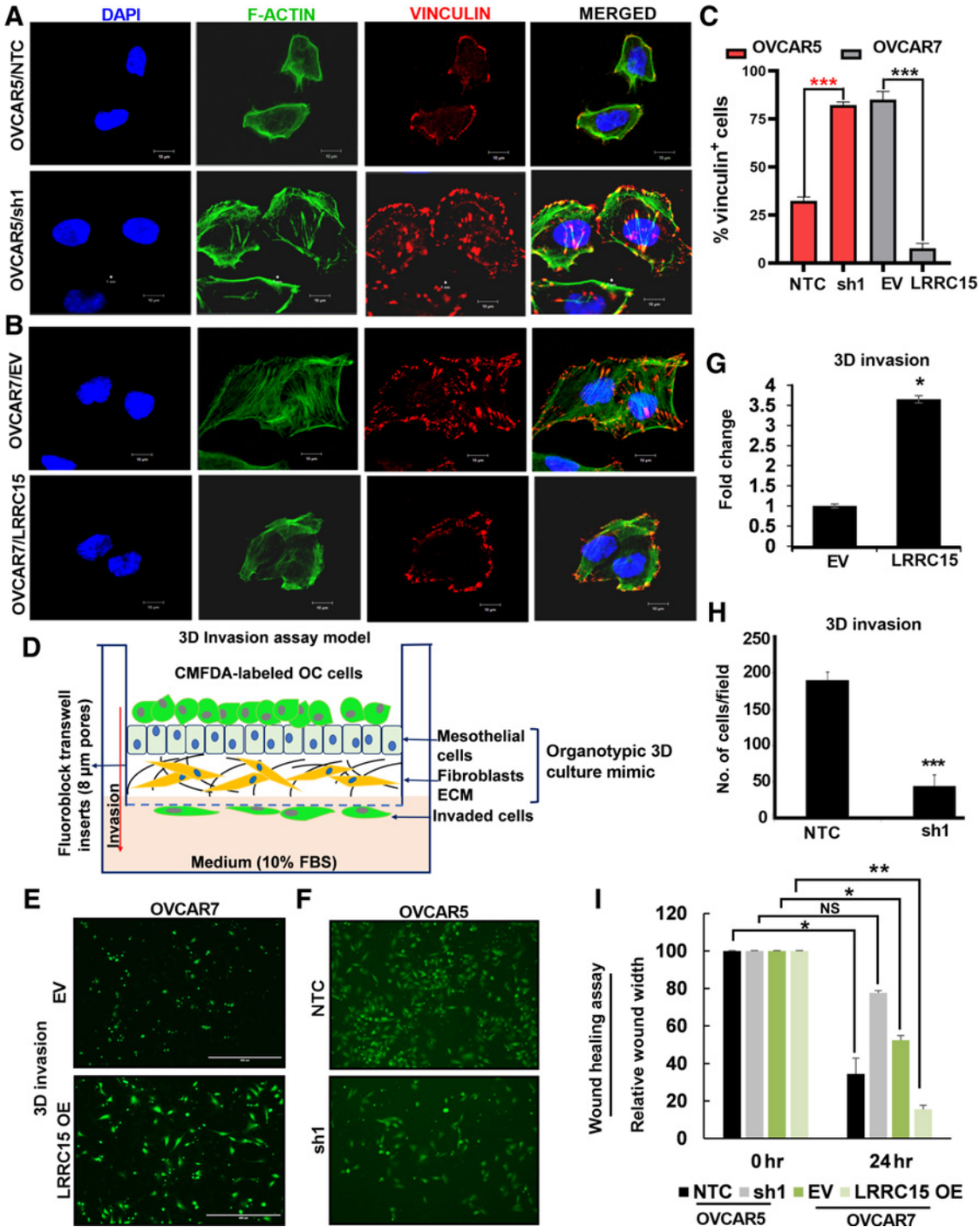

Figure 4.

Altered LRRC15 expression reveals distinct pattern of FA complex formation in ovarian cancer cells. **A,** OVCAR5 NTC and sh1 cells were grown on fibronectin-coated coverslips for 24 hours, followed by immunofluorescence study against F-actin (green) and vinculin (red) using the confocal microscopy. DAPI was used to stain the nucleus, and the merged images are represented. **B,** Similar immunofluorescence assay was performed in the OVCAR7 EV and LRRC15 OE cells, and the images are provided. Scale bar, 10 µm. **C,** Percentage of vinculin-positive cells in a total of 50 cells was counted and is represented as bar graph. **D,** Schematic representation of the invasion assay through the organotypic 3D culture model of the omentum surface. **E,** CMFDA-labeled EV control and LRRC15 OVCAR7 cells were allowed to invade the 3D culture matrix for 12 hours, and the representative images were provided. **F,** Similar invasion assay was performed in the OVCAR5 NTC and sh1 cells. **G–H,** Percent of invaded cells was scored for the 3D invasion assay and is presented as mean ± SEM, respectively. **I,** Wound healing assay was performed in the OVCAR5 NTC and sh1 cells, and in the EV control and LRRC15 OE OVCAR7 cells, the relative wound width was calculated using the ImageJ software and is represented. NS, not significant; *, $P < 0.05$; **, $P < 0.01$; ***, $P < 0.001$.

Having shown that LRRC15 promotes adherence to the omentum and alteration in FA formation, we determined if LRRC15 had a role in invading through the omentum surface in a 3D-culture model mimicking the surface layers of the omentum. The 3D-culture system was assembled by a confluent monolayer of human primary mesothelial cells seeded over a layer of type-I collagen and normal omental fibroblasts (**Fig. 4D**). Fluorescently labeled OVCAR5 NTC and KD cells and OVCAR7/LRRC15 and EV control cells were seeded on the 3D-culture matrix as previously described (33) and allowed to invade for 12 hours. A significant increase in invasion was obtained in the LRRC15/OVCAR7 cells compared with the vector control cells (**Fig. 4E** and **G**). In contrast, sh1 KD cells showed reduced invasion compared with control cells under similar assay conditions (**Fig. 4F** and **H**). Furthermore, LRRC15 OE OVCAR7 cells showed increased migration potential compared with EV control cells whereas the sh1 KD cells showed the reverse effect (**Fig. 4I**) in the wound-healing migration assay.

LRRC15 regulates multiple ECM gene expression and directly binds to β1-integrin

Among the well defined cell surface receptors that bind to various ECM proteins are integrins, particularly, α5β1-integrins in promoting metastasis in ovarian cancer are well recognized (34, 35). LRRC15 was necessary for binding to fibronectin, laminin, and collagen (Fig. 3G) and β1-integrin can heterodimerize with several α-subunits to form receptors for these three matrix (36). Moreover, FA formation involves integrin signaling mediated, at least in part, through engagement of β1-integrin. CD44, is another adhesion molecule that can bind to both fibronectin and collagen and associated with poor prognosis in patients with ovarian cancer (37, 38). Therefore, we studied the expression of β1-integrin and CD44 in OVCAR5 KD and NTC cells grown on FN-coated plates by flow cytometry. LRRC15-deficient OVCAR5 cells showed 80% downregulation of ITGB1 and 40% reduction in CD44 expression respectively compared with LRRC15 proficient control cells (**Fig. 5A–C**, Supplementary Fig. S2D and E).

Having found that there is a reduction in ITGB1 expression in the KD cells, we surmised that LRRC15 binding to FN in the ECM, may enhance ligand activation of β1-integrin by interacting with each other. Confocal microscopy revealed a reduction in the colocalization between LRRC15 with ITGB1 in KD cells compared with control cells, however, a strong interaction was observed in the OVCAR7/LRRC15 cells (**Fig. 5D–E**). The interaction was validated when LRRC15 coprecipitated with β1-integrin in the OVCAR5 NTC-control but not in -KD cells (**Fig. 5F**). Similar interaction was also obtained in the OVCAR7/LRRC15 cells compared with EV control (**Fig. 5G**). Consistent with these findings, the reverse immunoprecipitation against LRRC15 also immunoprecipitated β1-integrin in the OVCAR5/NTC and OVCAR7/LRRC15 cells (**Figs. 5F–G**, panel 3–4 respectively). To further validate the interaction, we performed the proximity-ligation assay to quantify the interaction between LRRC15 and ITGB1 in the above mentioned cell types (Supplementary Fig. S3A–B). A significant attenuation in the red fluorescent signal measuring positive interaction was obtained in the LRRC15 sh1 KD cells compared with the NTC cells (Supplementary Fig. S3A and C). In contrast the LRRC15 OE OVCAR7 cells showed more positive interaction compared with EV controls (Supplementary Fig. S3B and C).

LRRC15-β1 integrin interaction activates FA signaling

Given that LRRC15 associates with β1-integrin and KD cells have more vinculin-positive FA, we hypothesized that formation and deassembly of FAs that are in part regulated by FAK activity may be altered and reflective of the LRRC15 levels. OVCAR5 KD and NTC cells grown on FN did not show significant auto-phosphorylation of FAK at pY397 at 6 hours, whereas activation was observed in OVCAR7/LRRC15 cells (**Fig. 5H–I** respectively). The functional significance of the β1-integrin interaction with LRRC15 was investigated by assessing the effect of ITGB1 KO, which shows a reduction in migratory phenotype of the OVCAR5 cells (Supplementary Fig. S3D). LRRC15 KD and ITGB1 KO cells alone and in combination results in significant decrease in migration rate in ovarian cancer cells while the reverse is true in LRRC15-overexpressed cells and in the cells rescued for LRRC15 and ITGB1 in their respective KD cells (Supplementary Fig. S3E–F). To further validate, we performed adhesion assays on the scrambled (scr) control OVCAR5 cells expressing LRRC15 and ITGB1 KO OVCAR5 cells that still retain LRRC15 expression on FN-coated plates before and after preblocking the FN-binding sites with recombinant LRRC15 protein and mAb from AbbVie that is a strong binder of LRRC15. The data shows that preblocking LRRC15 binding to FN inhibits the adhesion of both LRRC15 expressing OVCAR5 NTC cells and ITGB1 KO cells that retain LRRC15 expression (Supplementary Fig. S3G–H).

Therapeutic targeting of LRRC15 suppresses omental/bowel metastasis in OVCAR5 xenograft model

We demonstrated that LRRC15 depletion led to suppression of both tumorigenesis and metastatic spread in xenograft model, implicating LRRC15 as a novel therapeutic target for ovarian cancer (6). Recently ABBV-085, an ADC-directed against LRRC15 was found to be safe and efficacious against LRRC15 cancer-positive and cancer-negative/stromal-positive preclinical models both as a monotherapy and/or in combination with standard therapies (9). To address the efficacy of ABBV-085 in ovarian cancer, we tested the effect of ABBV-085 *in vitro* in OVCAR5 cells. As shown in Fig. S4A–B, ABBV-085 dose-dependent reduction in cell viability was observed for LRRC15-expressing OVCAR5 NTC cells but not in KD cells.

To evaluate *in vivo* efficacy of ABBV-085 in suppressing early and late ovarian cancer metastasis, two different OVCAR5 xenograft models were used. In the early metastatic model (**Fig. 6A**) we evaluated the efficacy of ABBV-085 in preventing the adhesion of ovarian cancer cells to the omentum/peritoneum, where the therapy was initiated 3 days before ovarian cancer cell injection. As referred (9), after 3 days tumor cells were i.p. injected into female athymic nu/nu mice, followed by 5 doses of i.p. injections of ABBV-085 and the control drugs at an interval of every 3days. Treatment with ABBV-085 showed almost no tumor burden in the mice compared to the isotype-mAb and isotype-vc-MMAE drug-treated controls (**Figs. 6B–C**). Comparative analysis of tumor weight and mean abdominal circumference across the cohort also revealed the efficacy of ABBV-085 in preventing the adhesion of ovarian cancer cells compared to control groups (**Figs. 6D–E**). Reduced Ki67 staining was observed in the ABBV-085 treated group compared with controls (**Fig. 6F–G**).

Since majority of the ovarian cancer patients have widespread peritoneal dissemination and ascites at time of diagnosis, the efficacy of ABBV-085 was assessed after 1 week of tumor cell injection when they have had enough time to adhere to the peritoneal cavity. To determine if ABBV-085 can still be effective in inhibiting the micro-metastasis, in the late metastatic models, 6 doses each of ABBV-085 and the respective control drugs were administered at an interval of 3 days and the mice euthanized on day36 when the tumor burden exceeded 10% of the body weight in the control isotype-mAb cohort (Supplementary Fig. S5A). A significant regression of the metastatic growth was obtained in the ABBV-085 treated mice cohort compared

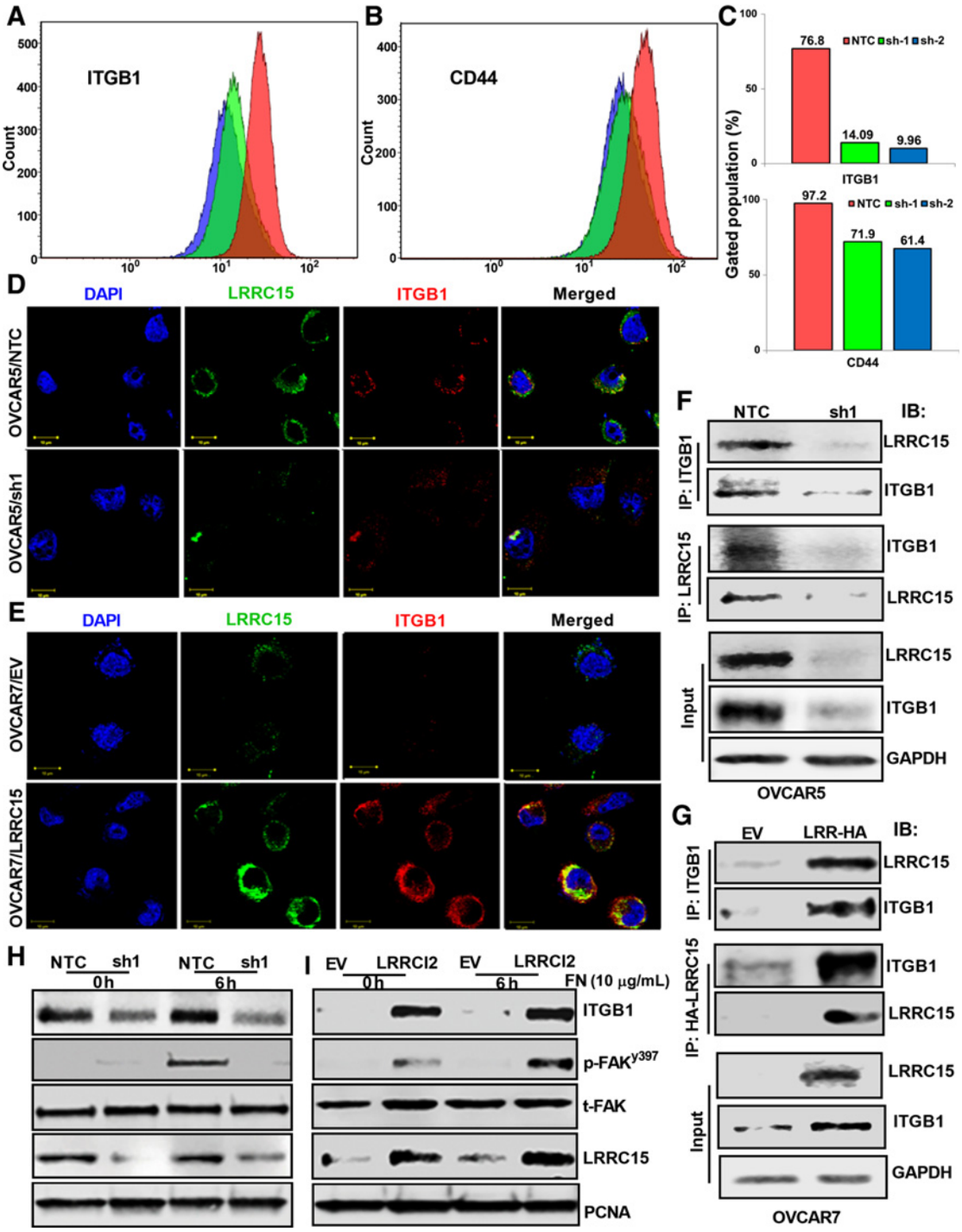

Figure 5.

β1-integrin–LRRC15 interaction activates the FAK signaling. **A** and **B,** OVCAR5 NTC, sh1, and sh2 cells were grown in fibronectin-coated plates for 24 hours, followed by flow cytometry analysis against fluorescently tagged ITGB1 and CD44. **C,** Percent of cells with positive signal was plotted. **D** and **E,** Colocalization studies between LRRC15 (green) and ITGB1 (red) in the OVCAR5 NTC and sh1 cells (**D**) and in the OVCAR7 EV and LRRCl5 cells (**E**) were evaluated using the confocal imaging. DAPI was used to stain the nucleus and the merged images are represented in both the cases. Scale bar, 10 μm. **F,** OVCAR5 NTC and sh1 cell extracts were immunoprecipitated with anti-ITGB1 and the coprecipitated LRRC15 was detected by Western blot analysis and vice versa. **G,** Similar immunoprecipitation studies were performed in the OVCAR7 EV and LRRC15 overexpressing cells. GAPDH was used as a loading control in both the cases. **H,** NTC and sh1 OVCAR5 cells were grown on FN-coated plates for 6 hours, followed by Western blot analysis. FAK pathway activation was performed by analyzing the p-FAK^{y397} and total FAK levels. h, hours. **I,** Similar immunoblot analysis of OVCAR7 EV and LRRC15 cells. Proliferating cell nuclear antigen (PCNA) was used for loading control. LRRC15 KD and OE was confirmed by probing against LRRC15 in the cell lysates, respectively.

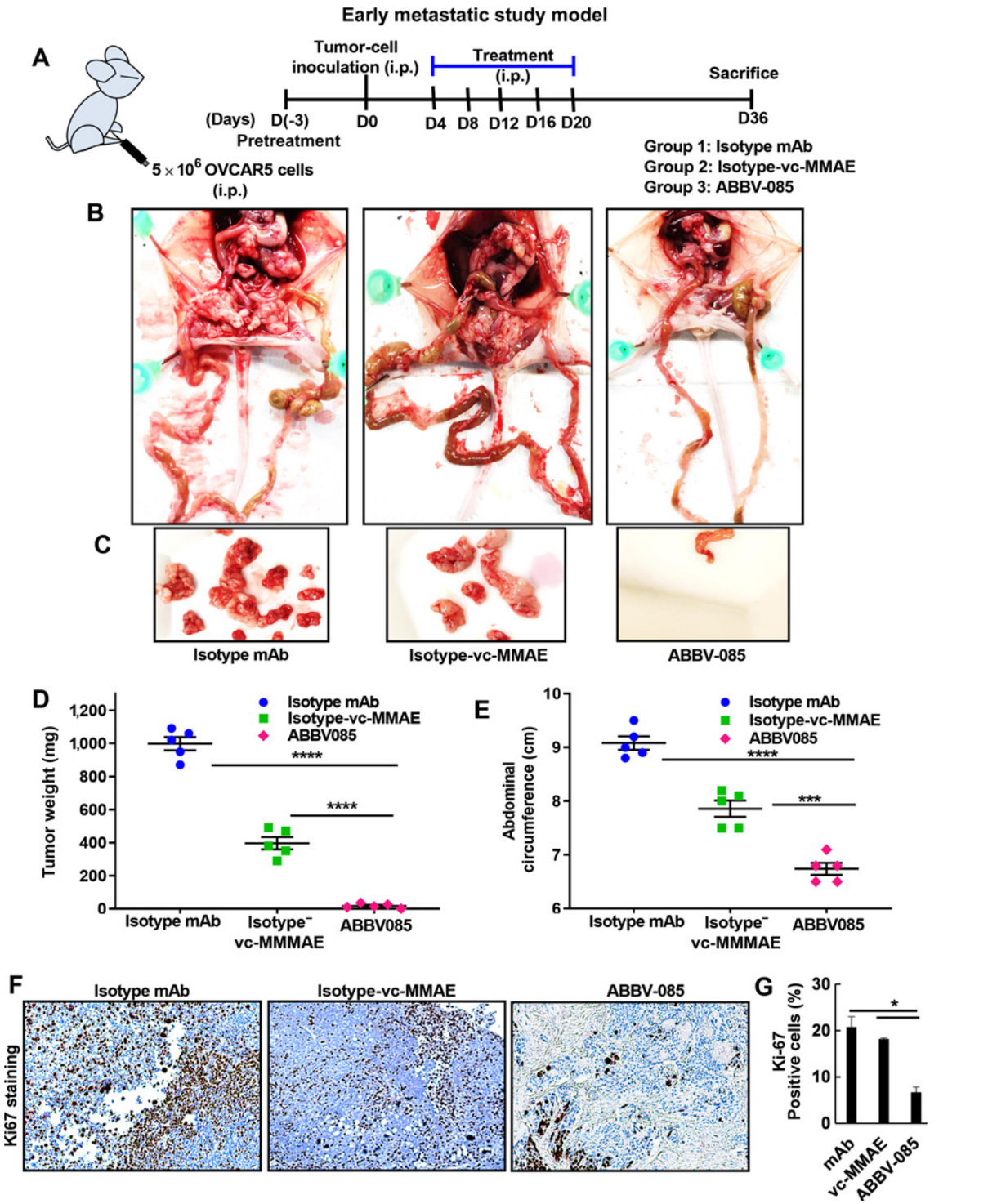

Figure 6.

ABBV-085 prevents peritoneal adhesion and inhibits tumor growth in early metastatic model of OVCAR5 xenografts. **A,** Schematic representation of the early metastatic study model in mice ovarian cancer xenograft. **B,** Pretreatment with control Isotype-mAb antibody (6 mg/kg), the Isotype-vc-MMAE-E2 drug control (6 mg/kg), and ABBV-085 (6 mg/kg) was initiated 3 days prior, followed by intraperitoneal OVCAR5 inoculation. Treatment was continued for 2 weeks as described previously and the animals were euthanized at day 36. Representative images of the mice with the tumor burden and metastatic nodes are shown. **C,** Representative images for the tumor burden per mice for the three treatment groups are provided. **D,** Graphical representation of the excised tumor weights in the 3 treatment cohorts. **E,** Abdominal circumference of each animal was measured on the day 36 across the treatment groups. **F,** Ki67 staining in each of the treated group was performed. **G,** Percent of Ki67-positive cells was quantified and is represented. *, $P < 0.05$; ***, $P < 0.001$; ****, $P < 0.0001$.

to the controls (Figs. S5B–C). However, isotype-vc-MMAE-E2 drug-control presented modest inhibitory side-effect mainly due to the highly cytotoxic nature of the drug in this model. Similar comparative analysis of tumor weight and mean abdominal circumference showed significant reduction in the metastatic dissemination and tumor growth in ABBV-085 treated mice (Figs. S5D–E) and reduction in Ki67 levels (Supplementary Fig. S5F–G). Liver histology as assessed by H&E staining were normal in control and treated groups in both the models (Supplementary Fig. S6A). Both the early and late metastatic model of ovarian cancer xenograft suggests that the targeted therapy of LRRC15-positive cancer cells with ABBV-085 prevents tumor growth.

ABBV-085 reduces cell viability in LRRC15 expressing human patient-derived ascites

To understand the clinical relevance, we screened the differential expression of LRRC15 in 7 patient-derived ascites cultures (17, 18) and the details of the clinical characteristics of the patients were given in the supplementary table S4. Confocal imaging of ascitic cultures using human epithelial specific antigen marker (EpCAM) and fibroblast activated protein marker (FAP) showed that ascitic cells are predominantly epithelial in nature (Supplementary Fig. S6B) and immunoblot analysis revealed that 4 of 7 samples A4832, A3626, JM067 and DC378 showed LRRC15 expression (**Fig. 7A**). To determine the efficacy of ABBV-085, the ascitic cells were cultured as 3D spheroids and treated in triplicates with indicated concentrations of ABBV-085 and the drug controls and cell viability was measured analyzing ATP levels using CellTiter-Glo. We observed a dose-dependent reduction in cell viability in the 4 LRRC15-expressing ascitic models upon ABBV-085 treatment compared to control drugs (**Fig. 7B–E**). However, no significant changes in the ATP levels were observed in the LRRC15 non-expressing A7683 and AM812 cells (**Fig. 7F–G**). Furthermore, CMFDA-labeled A4832 and AM812 ascites cells were seeded on top of fibronectin-coated plates for 2hr and percent adhered cells were counted upon treatment with ABBV-085 and drug controls. While LRRC15-positive A4832 cells showed a significant reduction in adhesion to fibronectin, however no such significant change was observed in adherence of LRRC15 non-expressing AM812 cells (Supplementary Fig. S6C–D). Additionally, western blot analysis on LRRC15 expressing ascites A4832 and JM067 showed no change in the expression of LRRC15 following treatment with isotype-mAb and MMAE-E2 controls and ABBV-085 (Supplementary Fig. S6E–F). Together it suggests that ABBV-085 treatment targets LRRC15 expressing ovarian cancer ascites.

Efficacy of ABBV-085 in the PDX model of ovarian cancer

Given the importance of targeting LRRC15 and the need for preclinical models to evaluate the efficacy of ABBV-085 in ovarian cancer, we selected the two PDX PH081 and PH127 models expressing LRRC15 (**Fig. 1E**) for our further studies. Since our *in vivo* adhesion model establishes that a time of 3hr is enough for the cells to adhere to peritoneum/omentum (**Fig. 3H–J**), we evaluated the efficacy of ABBV-085 in the pre-treatment metastatic PH127-PDX model. For the early metastatic model of PH127 xenograft, we found that only 3 mice out of 11 formed tumors in the ABBV-085 group (**Fig. 8A–B**) signifying the effect of ABBV-085 in inhibiting the adhesion of LRRC15 expressing cells to the peritoneum compared to 10 out of 11 and 9 out of 13 in isotype-vc-MMAE and mAb controls respectively. A detailed analysis at the initial time of detectable tumor engraftment by ultrasound also showed similar effect in the PH127 xenograft and Ki67 staining also showed reduced expression in the ABBV-085 treated group (**Fig. 8C**, Supplementary Fig. S7A–B). Decreased p-FAK^{y397} levels and a reduction in ECM infiltration was found in ABBV-085 treated cohort compared to controls (Supplementary Figs. S7C–D). Additionally, western analysis of LRRC15 showed that there is no change in the expression of LRRC15 itself within the ABBV-085 treated and drug control treated groups (Supplementary Fig. S7E). No toxicity was also observed in the ABBV-085 treated group compared to the drug control groups by analyzing the liver histology (Supplementary Fig. S7F).

We also determined the efficacy of ABBV-085 in both early and late metastatic model for PH081 PDX. For the early metastatic model of PH081 xenograft, treatment was initiated 3days prior to tumor cell injection followed by 6 doses of treatment at an interval of 4days (**Fig. 8D**). The tumor volume was measured for 15weeks by ultrasound. A significant regression in tumor volume was observed in ABBV-085 treated animal cohort by week 8 compared to two control groups (**Fig. 8E**). For the late metastatic model, 6 doses of treatment at an interval of 4days were started after 2weeks of tumor cell injection when the tumors reached 0.5–1 cm^2 and mice were monitored for reduction in tumor volume for 6weeks. To our surprise, there was no difference in tumor growth in ABBV-085 treated cohort compared to controls (**Fig. 8F**). ABBV-085 treated cohort showed reduced Ki67 levels in the PH081 early metastatic model (Supplementary Fig. S8A–B). However, no adverse effects like weight loss or poor health due to treatments was noted in all the PDX models. Similar decreased levels of p-FAK^{y397} and reduced ECM infiltration was found in ABBV-085 treated cohort compared to controls (Supplementary Fig. S8C–D). Furthermore, immunoblot analysis of LRRC15 showed no change in the expression between the ABBV-085–treated and drug control–treated groups (Supplementary Fig. S8E). Additionally the hematoxylin and eosin (H&E) staining of the tumor tissue on the omentum from PH081 PDX model show that tumor cells were able to adhere and form tumors (Supplementary Fig. S8F). Together, the result strongly supports that ABBV-085 effectively prevents adhesion and *de novo* tumor growth but may not suppress the previously established tumors.

Discussion

Metastasis is the most significant step in cancer progression as it limits the curative surgical treatment for ovarian cancer. Due to the essential nature of cell–to–cell adhesion, cell–to–matrix adhesion, and resistance to anoikis in successful metastatic progression, critical regulators that control these steps may play an important role in ovarian cancer dissemination. A better understanding of the regulators of various steps in omental/bowel metastasis in ovarian cancer is essential to clinically facilitate therapeutic approaches that will treat this deadly complication and improve patient prognosis.

Our recent interest in identifying regulators that promotes metastasis to the bowel/omentum in ovarian cancer revealed a specific metastatic gene signature ($n = 21$ genes) using RNA sequencing analysis. Among the most significantly overexpressed genes in bowel metastases, we found that 13 of the 21 ECM-related genes expressed only in the stroma, with an exception of LRRC15, which was found to be present both in stroma and epithelial compartments (6). Increasing evidence showed that most of these genes were associated with regulation of EMT, fibrosis, and metastasis. For example, reports revealed that MFAP5 coordinates binding to $\alpha5\beta3$ integrin and activates collagen genes through ERK signaling in CAFs (39, 40). Additionally, stromal expression of fibroblast activating protein, FAP (41), COL11A1, and POSTN1 emphasizes the significance of the stromal component in the metastatic development (42). Affymetrix GeneChip of breast tumors showed high differential *LRRC15*

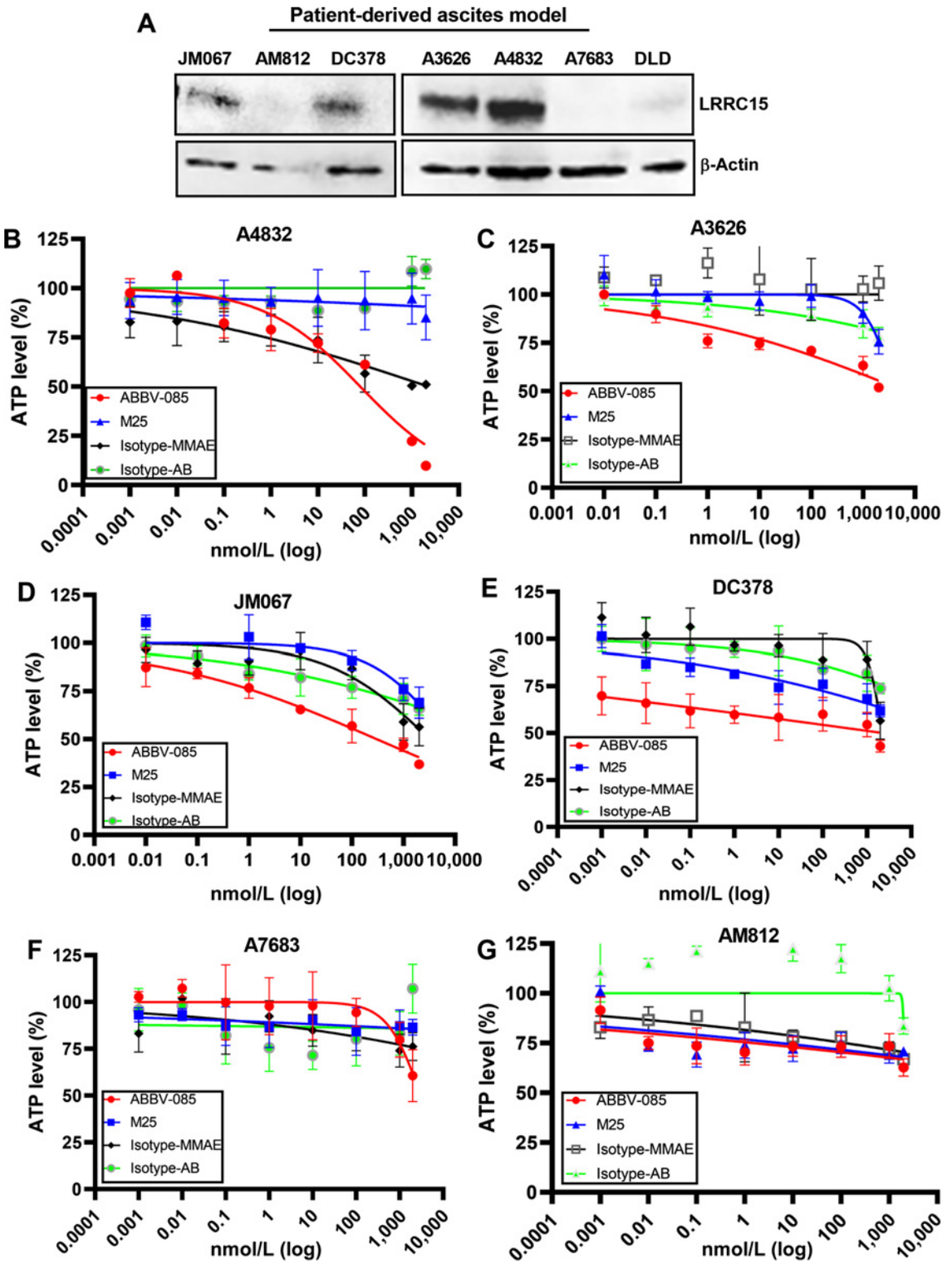

Figure 7.

Treatment with ABBV-085 reduces cell viability in LRRC15-expressing human patient-derived ascites. **A,** Analysis of LRRC15 expression in 7 human patient-derived ascites. β-actin was shown as a loading control. **B–G,** Percent ATP level was analyzed upon treatment with ABBV-085 and drug controls in LRRC15 expressing A4832 (**B**), A3626 (**C**), JM067 (**D**), DC378 and LRRC15 (**E**), nonexpressing A7683 (**F**), and AM812 ascites (**G**) cells.

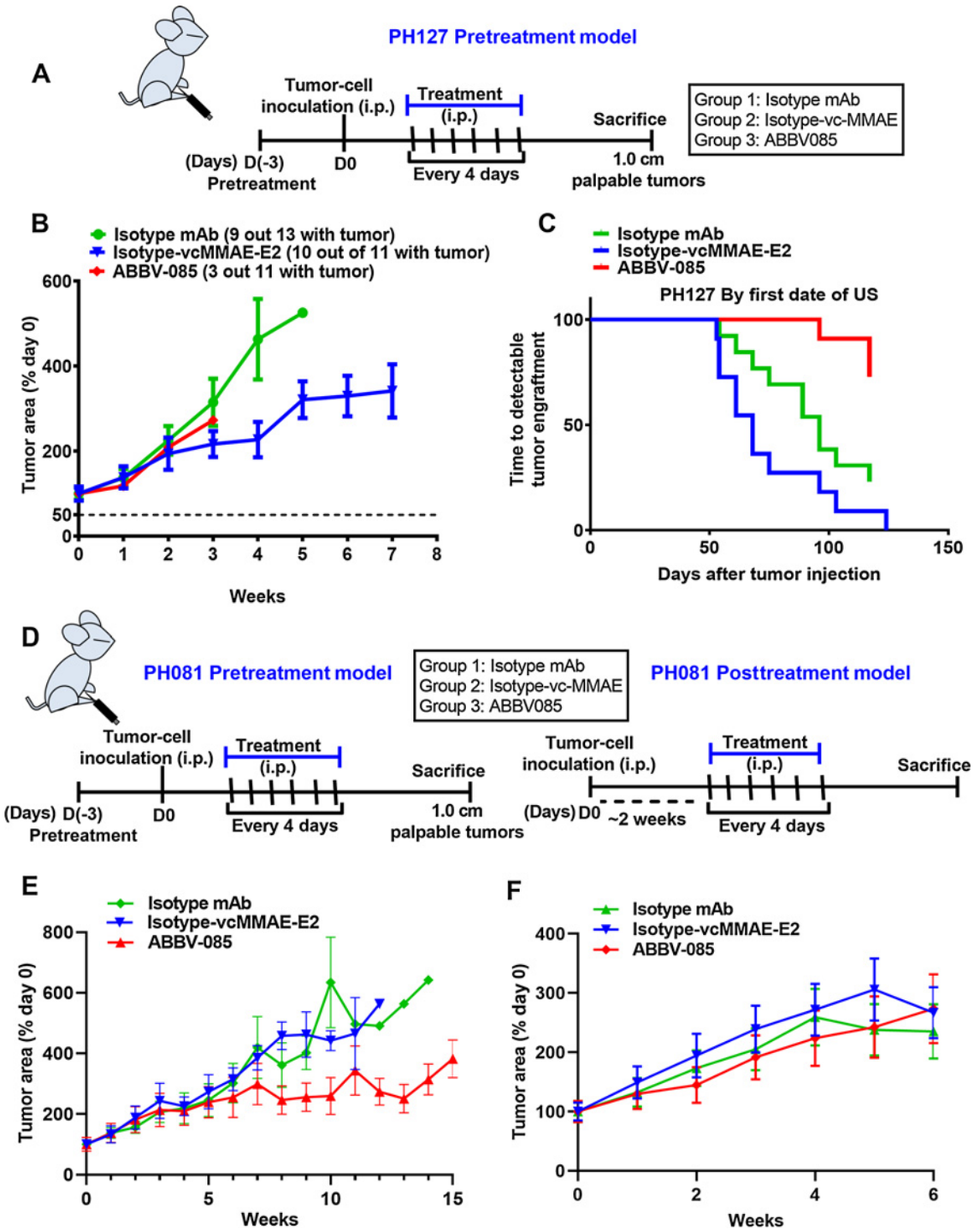

Figure 8.

Therapeutic efficacy of ABBV-085 in the PH127 and PH081 ovarian cancer PDX xenograft model. **A,** Schematic representation of the early metastatic model of PH127 PDX xenograft. **B,** Percent change in tumor area in PH127 PDX early metastatic model following treatments with ABBV-085 and control drugs as determined by ultrasound weekly. **C,** Graphical analysis of the time required for the detectable tumor engraftment in each mouse from the three treatment cohorts. **D,** Schematic representation of PH081 PDX in the pre- and posttreatment models. **E** and **F,** Percent change in tumor area in the PH081 PDX early metastatic model (**E**) and in the late metastatic model (**F**) following treatments with the drugs as determined by ultrasound weekly.

expression in cells metastasizing to the bone compared with the brain (43). Bignotti and colleagues reported *LRRC15* as one of the upregulated genes in omental mets amongst 120 genes compared with unmatched ovarian cancer (44) and studies by Reynolds and colleagues (45), showed that LRRC15 binds to ECM proteins including collagen and fibronectin. However, whether LRRC15 has a crucial role to play in the metastatic cascade of ovarian cancer was never explored. In this study, we identified LRRC15 as playing a significant role in ovarian cancer metastasis by promoting anoikis resistance, increased adhesion, and colonization to omentum/peritoneum and invasion using different approaches. Mechanistically we report for the first time that in ovarian cancer, LRRC15-expressing cells adhere to fibronectin and promote the clustering of β1-integrin followed by the activation of FAK signaling and promote metastasis.

Among the stromal markers, Yeung and colleagues showed that targeting using MFAP5 ADC reduces fibrosis and increases chemosensitivity in both the ovarian and pancreatic cancers (39). Additional report by Fabre and colleagues showed that targeting FAP with OMTX705 ADC prevents tumor growth supporting its clinical development (46). However, clinical development of these ADCs is still warranted. In contrast, LRRC15-targeting ADC, ABBV-085 was evaluated in phase I clinical trial in sarcomas and other advanced solid tumors (NCT02565758; ref. 47). Promising antitumor efficacy was obtained when ABBV-085 was used as monotherapy or in combination therapy in xenograft models of several solid tumors including sarcoma, pancreatic, head and neck, breast, glioblastoma, and lung (9). Additionally, ABBV-085 monotherapy attenuates tumor growth in LRRC15-positive soft-tissue sarcoma (STS) PDX models (48) including the highly chemo-refractive undifferentiated pleomorphic sarcomas (UPS) with poor survival rate and treatment options (49). Our *in vivo* analysis for the first time showed the efficacy of targeting LRRC15 by ABBV-085 in preventing the adhesion and inhibiting metastasis of LRRC15-expressing cancer cells using both the OVCAR5-based early and late metastatic xenograft models. Additionally, ABBV-085 treatment inhibits tumor burden and dissemination in the early metastatic model of both the LRRC15-positive PH127 and PH081 PDX xenograft and validates that ABBV-085 prevents early adhesion phenomenon of the cancer cells required for metastatic dissemination.

However, to our surprise, we found no difference in tumor growth in ABBV-085–treated cohort compared with the two control groups in the late metastatic model of the PH081 xenograft. The reason for this unexpected finding is, we believe is the propensity of cancer cells to seed in the peritoneal/omental/bowel may occur within a day or two allowing these micrometastases to start growing at the rate to reach a tumor volume after 2 weeks when the drug treatment was initiated. The seeding of the micrometastatic tumors may have counteracted the effect of ABBV-085 to prevent adhesion of LRRC15-expressing cells to the preferred "soil". Treatment with ABBV-085 may have targeted LRRC15-expressing clones, however due to the long latent period and tumor heterogeneity the LRRC15 nonexpressing clones may have survived in this favorable environment and overgrew once the LRRC15-expressing cells were eliminated. Taken together, the result suggests that ABBV-085 is able to prevent adhesion of tumor cells when the mice were pretreated with the drug.

Our additional studies showed promising antitumor efficacy with ABBV-085 in the LRRC15-positive ovarian cancer ascites cells while no effect in LRRC15 nonexpressing cells. One of the arguments against targeting proteins overexpressed in metastatic sites of ovarian cancer is that, the majority of tumors on the omentum and the ovary are optimally debulked and therefore targeting them may have negligible clinical significance. However, it does not take into account the presence of minimal residual disease (MRD) that potentially results in recurrent disease. Due to its unique tumor biology, which is initially dependent on attachment to a fibronectin-rich mesothelial surface, ovarian cancer may be especially suited to a LRRC15–targeting approach.

Tumor-stromal interaction that contributes to inherent and acquired multidrug resistance is the major reason for chemotherapy failure in most cancers (49, 50). Thus, improvement of antifibrotic/antistromal therapies was in development and LRRC15 as a mesenchymal marker should be potentially exploitable in solid tumor therapy. Our data demonstrates that ABBV-085 is highly effective in treating micrometastases and in killing tumor cells in ascites. Since most patients with ovarian cancer suffer from relapse and development of ascites, following the standard-of-care cytoreductive surgery and chemotherapy, ABBV-085 can be effective in prevention of such conditions. Till date, analysis on the expression of LRRC15 in relation to recurrent and MRD is missing and is associated with poor survival. Identification of MRD biomarkers is critical specifically if they are drugable targets such as LRRC15 and may lead to effective treatment. As we continue to develop an improved understanding of the complex interactions in the microenvironment, we will be able to advance stroma-targeting strategies for more effective anticancer treatments.

Authors' Disclosures

S.J. Weroha reports personal fees from AstraZeneca; nonfinancial support from ProLynx; and personal fees from Kiyatec outside the submitted work; in addition, S.J. Weroha has a patent for Ovarian PDX with royalties paid. J.W. Purcell reports other support from AbbVie during the conduct of the study; other support from AbbVie outside the submitted work; in addition, J.W. Purcell has a patent for ANTI-huLRRC15 ANTIBODY DRUG CONJUGATES AND METHODS FOR THEIR USE issued; and is an employee and stockholder of AbbVie. S.H. Kaufmann reports grants from NCI during the conduct of the study and grants from Takeda outside the submitted work. No disclosures were reported by the other authors.

Authors' Contributions

U. Ray: Formal analysis, validation, investigation, methodology, writing–original draft. **D.-B. Jung:** Formal analysis, validation, investigation, methodology. **L. Jin:** Investigation, methodology. **Y. Xiao:** Investigation. **S. Dasari:** Investigation, methodology. **S. Sarkar Bhattacharya:** Investigation. **P. Thirusangu:** Methodology, writing–review and editing. **J.K. Staub:** Methodology. **D. Roy:** Methodology. **B. Roy:** Investigation. **S.J. Weroha:** Investigation, methodology. **X. Hou:** Validation, investigation, methodology. **J.W. Purcell:** Resources, project administration, writing–review and editing. **J.N. Bakkum-Gamez:** Resources, writing–review and editing. **S.H. Kaufmann:** Resources, writing–review and editing. **N. Kannan:** Writing–review and editing. **A.K. Mitra:** Supervision, investigation, methodology, writing–review and editing. **V. Shridhar:** Conceptualization, resources, supervision, funding acquisition, project administration, writing–review and editing.

Acknowledgments

This work is supported in part by the grants from the Minnesota Ovarian Cancer Alliance and the Department of Experimental Pathology and Laboratory Medicine and the Mayo Clinic (V. Shridhar) and the NIH (grant no. P50CA136393 for providing the ascites cells from patients wih ovarian cancer. The authors acknowledge the support from Dr. A.K. Mitra [DoD OCRP Ovarian Cancer Academy Award (W81XWH-15-0253) and American Cancer Society (RSG-21-019-01-CSM)]. The authors thank Drs. Amy Skubitz and Kristin Boylan for providing the cryopreserved patient-derived ascites samples from the University of Minnesota, Minneapolis under an IRB-approved protocol. The normal FTE cells were obtained from Dr. Ronny Drapkin, University of Pennsylvania, Philadelphia, PA; NOF151hTERT cells, HeyA8, and HeyA8MDR cells were obtained from MD Anderson Cancer Center, Houston, TX; PEO 1/4 from Dr. Taniguchi, Fred Hutchinson Cancer Research Center, Seattle, Washington; OVCAR 8/4 cells from Fox Chase Cancer Center, Philadelphia, PA; LP9/TERT-1 mesothelial cells from Coriell Institute for Medical Research,

Camden, NJ; immortalized ovarian surface epithelium IOSE523 from Dr. Nelly Auersperg, UBC; OV202 cells from Dr. Cheryl A. Conover, Mayo Clinic, Rochester, MN; SKOV3 and its derivatives from Dr. Michael Seiden, Massachusetts General Hospital, Boston, MA on MTA; and OVCAR 7/5/10 and TOV21G from ATCC. The authors acknowledge contributions of the Pathology Research Core laboratory, the Microscopy Core laboratory, and the Flow Cytometry Facility, Mayo Clinic.

The costs of publication of this article were defrayed in part by the payment of page charges. This article must therefore be hereby marked *advertisement* in accordance with 18 U.S.C. Section 1734 solely to indicate this fact.

Received March 5, 2021; revised July 21, 2021; accepted October 12, 2021; published first October 15, 2021.

References

1. Siegel RL, Miller KD, Jemal A. Cancer statistics, 2020. CA Cancer J Clin 2020;70:7–30.
2. Paul Olson TJ, Pinkerton C, Brasel KJ, Schwarze ML. Palliative surgery for malignant bowel obstruction from carcinomatosis: a systematic review. JAMA Surg 2014;149:383–92.
3. Mangili G, Aletti G, Frigerio L, Franchi M, Panacci N, Viganò R, et al. Palliative care for intestinal obstruction in recurrent ovarian cancer: a multivariate analysis. Int J Gynecol Cancer 2005;15:830–5.
4. Lengyel E. Ovarian cancer development and metastasis. Am J Pathol 2010;177:1053–64.
5. Feuer DJ, Broadley KE, Shepherd JH, Barton DP. Surgery for the resolution of symptoms in malignant bowel obstruction in advanced gynaecological and gastrointestinal cancer. Cochrane Database Syst Rev 2000:Cd002764.
6. Mariani A, Wang C, Oberg AL, Riska SM, Torres M, Kumka J, et al. Genes associated with bowel metastases in ovarian cancer. Gynecol Oncol 2019;154:495–504.
7. Kobe B, Deisenhofer J. The leucine-rich repeat: a versatile binding motif. Trends Biochem Sci 1994;19:415–21.
8. Kobe B, Kajava A. The leucine-rich repeat as a protein recognition motif. Curr Opin Struct Biol 2001;11:725–32.
9. Purcell JW, Tanlimco SG, Hickson J, Fox M, Sho M, Durkin L, et al. LRRC15 is a novel mesenchymal protein and stromal target for antibody-drug conjugates. Cancer Res 2018;78:4059–72.
10. Stanbrough M, Bubley GJ, Ross K, Golub TR, Rubin MA, Penning TM, et al. Increased expression of genes converting adrenal androgens to testosterone in androgen-independent prostate cancer. Cancer Res 2006;66:2815–25.
11. Satoh K, Hata M, Shimizu T, Yokota H, Akatsu H, Yamamoto T, et al. Lib, transcriptionally induced in senile plaque-associated astrocytes, promotes glial migration through extracellular matrix. Biochem Biophys Res Commun 2005;335:631–6.
12. Bierkens M, Krijgsman O, Wilting SM, Bosch L, Jaspers A, Meijer GA, et al. Focal aberrations indicate EYA2 and hsa-miR-375 as oncogene and tumor suppressor in cervical carcinogenesis. Genes Chromosomes Cancer 2013;52:56–68.
13. Satoh K, Hata M, Yokota H. High lib mRNA expression in breast carcinomas. DNA Res 2004;11:199–203.
14. Schuetz CS, Bonin M, Clare SE, Nieselt K, Sotlar K, Walter M, et al. Progression-specific genes identified by expression profiling of matched ductal carcinomas in situ and invasive breast tumors, combining laser capture microdissection and oligonucleotide microarray analysis. Cancer Res 2006;66:5278–86.
15. Cheung M, Pei J, Pei Y, Jhanwar SC, Pass HI, Testa JR. The promyelocytic leukemia zinc-finger gene, PLZF, is frequently downregulated in malignant mesothelioma cells and contributes to cell survival. Oncogene 2010;29:1633–40.
16. Rattan R, Narita K, Chien J, Maguire JL, Shridhar R, Giri S, et al. TCEAL7, a putative tumor suppressor gene, negatively regulates NF-kappaB pathway. Oncogene 2010;29:1362–73.
17. Burleson KM, Boente MP, Pambuccian SE, Skubitz AP. Disaggregation and invasion of ovarian carcinoma ascites spheroids. J Transl Med 2006;4:6.
18. Burleson KM, Casey RC, Skubitz KM, Pambuccian SE, Oegema TR Jr., Skubitz AP, et al. Ovarian carcinoma ascites spheroids adhere to extracellular matrix components and mesothelial cell monolayers. Gynecol Oncol 2004;93:170–81.
19. Sarkar Bhattacharya S, Thirusangu P, Jin L, Roy D, Jung D, Xiao Y, et al. PFKFB3 inhibition reprograms malignant pleural mesothelioma to nutrient stress-induced macropinocytosis and ER stress as independent binary adaptive responses. Cell Death Dis 2019;10:725.
20. Guzmán C, Bagga M, Kaur A, Westermarck J, Abankwa D. ColonyArea: an ImageJ plugin to automatically quantify colony formation in clonogenic assays. PLoS One 2014;9:e92444.
21. Ray U, Roy Chowdhury S, Vasudevan M, Bankar K, Roychoudhury S, Roy SS. Gene regulatory networking reveals the molecular cue to lysophosphatidic acid-induced metabolic adaptations in ovarian cancer cells. Mol Oncol 2017;11:491–516.
22. Dasari S, Pandhiri T, Grassi T, Visscher DW, Multinu F, Agarwal K, et al. Signals from the Metastatic Niche Regulate Early and Advanced Ovarian Cancer Metastasis through miR-4454 Downregulation. Mol Cancer Res 2020;18:1202–17.
23. Menon V, Thomas R, Ghale AR, Reinhard C, Pruszak J. Flow cytometry protocols for surface and intracellular antigen analyses of neural cell types. J Vis Exp 2014.
24. Weroha SJ, Becker MA, Enderica-Gonzalez S, Harrington SC, Oberg AL, Maurer MJ, et al. Tumorgrafts as in vivo surrogates for women with ovarian cancer. Clin Cancer Res 2014;20:1288–97.
25. Zhang Q, Hou X, Evans BJ, VanBlaricom JL, Weroha SJ, Cliby WA. LY2157299 Monohydrate, a TGF-βR1 Inhibitor, Suppresses Tumor Growth and Ascites Development in Ovarian Cancer. Cancers (Basel) 2018;10.
26. Tan DS, Agarwal R, Kaye SB. Mechanisms of transcoelomic metastasis in ovarian cancer. Lancet Oncol 2006;7:925–34.
27. Shield K, Ackland ML, Ahmed N, Rice GE. Multicellular spheroids in ovarian cancer metastases: Biology and pathology. Gynecol Oncol 2009;113:143–8.
28. Kenny HA, Kaur S, Coussens LM, Lengyel E. The initial steps of ovarian cancer cell metastasis are mediated by MMP-2 cleavage of vitronectin and fibronectin. J Clin Invest 2008;118:1367–79.
29. Jockusch BM, Rüdiger M. Crosstalk between cell adhesion molecules: vinculin as a paradigm for regulation by conformation. Trends Cell Biol 1996;6:311–5.
30. Zamir E, Geiger B. Molecular complexity and dynamics of cell-matrix adhesions. J Cell Sci 2001;114:3583–90.
31. Ziegler WH, Liddington RC, Critchley DR. The structure and regulation of vinculin. Trends Cell Biol 2006;16:453–60.
32. Mitra AK, Chiang CY, Tiwari P, Tomar S, Watters KM, Peter ME, et al. Microenvironment-induced downregulation of miR-193b drives ovarian cancer metastasis. Oncogene 2015;34:5923–32.
33. Kenny HA, Lal-Nag M, White EA, Shen M, Chiang CY, Mitra AK, et al. Quantitative high throughput screening using a primary human three-dimensional organotypic culture predicts in vivo efficacy. Nat Commun 2015;6:6220.
34. Sawada K, Ohyagi-Hara C, Kimura T, Morishige K. Integrin inhibitors as a therapeutic agent for ovarian cancer. J Oncol 2012;2012:915140.
35. Sawada K, Mitra AK, Radjabi AR, Bhaskar V, Kistner EO, Tretiakova M, et al. Loss of E-cadherin promotes ovarian cancer metastasis via alpha 5-integrin, which is a therapeutic target. Cancer Res 2008;68:2329–39.
36. Humphries JD, Byron A, Humphries MJ. Integrin ligands at a glance. J Cell Sci 2006;119:3901–3.
37. Annabi B, Thibeault S, Moumdjian R, Béliveau R. Hyaluronan cell surface binding is induced by type I collagen and regulated by caveolae in glioma cells. J Biol Chem 2004;279:21888–96.
38. Wirth F, Lubosch A, Hamelmann S, Nakchbandi IA. Fibronectin and its receptors in hematopoiesis. Cells 2020;9:2717.
39. Yeung TL, Leung CS, Yip KP, Sheng J, Vien L, Bover LC, et al. Anticancer immunotherapy by MFAP5 blockade inhibits fibrosis and enhances chemosensitivity in ovarian and pancreatic cancer. Clin Cancer Res 2019;25:6417–28.
40. Li Q, Zhang Y, Jiang Q. MFAP5 suppression inhibits migration/invasion, regulates cell cycle and induces apoptosis via promoting ROS production in cervical cancer. Biochem Biophys Res Commun 2018;507:51–8.
41. Teichgräber V, Monasterio C, Chaitanya K, Boger R, Gordon K, Dieterle T, et al. Specific inhibition of fibroblast activation protein (FAP)-alpha prevents tumor progression in vitro. Adv Med Sci 2015;60:264–72.
42. Zhang Q, Wang C, Cliby WA. Cancer-associated stroma significantly contributes to the mesenchymal subtype signature of serous ovarian cancer. Gynecol Oncol 2019;152:368–74.

43. Klein A, Olendrowitz C, Schmutzler R, Hampl J, Schlag PM, Maass N, et al. Identification of brain- and bone-specific breast cancer metastasis genes. Cancer Lett 2009;276:212–20.
44. Bignotti E, Tassi RA, Calza S, Ravaggi A, Bandiera E, Rossi E, et al. Gene expression profile of ovarian serous papillary carcinomas: identification of metastasis-associated genes. Am J Obstet Gynecol 2007;196:245.e1–11.
45. Reynolds PA, Smolen GA, Palmer RE, Sgroi D, Yajnik V, Gerald WL, et al. Identification of a DNA-binding site and transcriptional target for the EWS-WT1(+KTS) oncoprotein. Genes Dev 2003;17:2094–107.
46. Fabre M, Ferrer C, Domínguez-Hormaetxe S, Bockorny B, Murias L, Seifert O, et al. OMTX705, a novel FAP-Targeting ADC demonstrates activity in chemotherapy and pembrolizumab-resistant solid tumor models. Clin Cancer Res 2020;26:3420–30.
47. Ben-Ami E, Perret R, Huang Y, Courgeon F, Gokhale PC, Laroche-Clary A, et al. LRRC15 targeting in soft-tissue sarcomas: biological and clinical implications. Cancers (Basel) 2020;12.
48. Savina M, Le Cesne A, Blay JY, Ray-Coquard I, Mir O, Toulmonde M, et al. Patterns of care and outcomes of patients with METAstatic soft tissue SARComa in a real-life setting: the METASARC observational study. BMC Med 2017;15:78.
49. Marin JJ, Sanchez de Medina F, Castaño B, Bujanda L, Romero MR, Martinez-Augustin O, et al. Chemoprevention, chemotherapy, and chemoresistance in colorectal cancer. Drug Metab Rev 2012;44:148–72.
50. Qu Y, Dou B, Tan H, Feng Y, Wang N, Wang D. Tumor microenvironment-driven non-cell-autonomous resistance to antineoplastic treatment. Mol Cancer 2019;18:69.